RSC Advances

PAPER

View Article Online
View Journal | View Issue

Cite this: *RSC Adv.*, 2026, **16**, 27212

The cocrystals of isorhamnetin and isoliquiritigenin with 4,4′-bipyridine: system characterization, stability, dissolution and anticancer activity

Yu Liu,[a] Jian Lei,[a] Ting Li,[a] Aiyu Zhong,[a] Zihan Zhu,[a] Junxiao Lu,[a] Zhipeng Wang, *[a] Panpan Zhao*[b] and Zhigang Wu*[a]

Received 8th March 2026
Accepted 5th May 2026

DOI: 10.1039/d6ra01981a

rsc.li/rsc-advances

As two natural products, isorhamnetin and isoliquiritigenin have been demonstrated to have significant anticancer activity. However, various pharmaceutical defects, such as low solubility and poor bioavailability, impede their anticancer efficacy. To optimize the anticancer efficacy of isorhamnetin and isoliquiritigenin, a scientific cocrystal design was performed to obtain two newly prepared cocrystals in this study. Leveraging multiple analytical techniques including single-crystal X-ray diffraction, powder X-ray diffraction, Fourier transform infrared spectroscopy, differential scanning calorimetry and thermogravimetric analysis, the isorhamnetin-4,4′-bipyridine (2 : 3) and isoliquiritigenin-4,4′-bipyridine (1 : 1) cocrystals were systematically characterized. The results of a series of evaluations on their stabilities, dissolution and anticancer activities demonstrated that these two cocrystals could remain stable under three different extreme environments, and the isorhamnetin-4,4′-bipyridine (2 : 3) cocrystal achieved significant improvement in solubility, dissolution rate and anticancer efficacy compared to isorhamnetin. For the isoliquiritigenin-4,4′-bipyridine (1 : 1) cocrystal, there was no increase in its solubility and dissolution rate compared to isoliquiritigenin. Nevertheless, a slight increase in the anticancer activity of isoliquiritigenin was achieved by the formation of the cocrystal. This study was a meaningful investigation, which not only laid an innovative material foundation for the development of isorhamnetin and isoliquiritigenin but also provided a new strategy to optimize the pharmaceutical properties of natural products.

Introduction

With the characteristics of complex mechanisms, high mortality rates, poor cure rates, great risk of recurrence, lengthy treatment cycles and expensive treatment costs, cancer is a major disease threatening human life and health.[1] Cancer is undoubtedly devastating the health and quality of life of countless patients. Recently, the number of cancer patients has been steadily increasing and showing a trend toward increased prevalence in the youth population, mainly due to unhealthy lifestyle habits and the impact of food and living environments; given the acceleration of population aging, this trend is concerning.[2,3] Although there are different kinds of anticancer drugs available, a lot of chemotherapeutic agents induce significant toxic side effects and drug resistance during treatment, severely hindering the therapeutic progress and efficacy for cancer patients.[4–6] Therefore, the development of highly effective and low-toxicity anticancer drugs is extremely urgent.

To the best of our knowledge, natural products constitute a vital treasure trove of pharmaceuticals and serve as a crucial source for drug development. Due to mild and sustained pharmacological effects, minimal adverse reactions as well as the multi-targeted, multi-effect and multifunctional mechanisms of action inherent in natural products, developing new anticancer drugs from natural products holds significant research value.[7,8] As a kind of indispensable natural bioactive compound, flavonoids are widely distributed in nature and exhibit numerous pharmacological effects with well-established therapeutic activity and low toxicity.[9] It is reported that flavonoids exhibit various significant pharmacological activities, such as antioxidant, antibacterial, antiviral, anti-stress, anti-tumor, analgesic, anti-inflammatory, immunomodulatory and so on.[10–12] Isorhamnetin (IRN, Fig. 1a) and isoliquiritigenin (ISL, Fig. 1b) are two typical flavonoid compounds, and they are found to have significant anticancer activity. According to previous studies, IRN exerts anticancer activity through inhibiting tumor cell proliferation, promoting tumor cell apoptosis, suppressing tumor cell migration and invasion, inhibiting oncogene expression and enhancing tumor suppressor gene

[a]*Hebei Key Laboratory of Neuropharmacology, Department of Pharmacy, Hebei North University, Zhangjiakou, 075000, China. E-mail: wangzp0128@sina.com; wuzhigang1982@126.com*

[b]*Department of Endocrinology and Metabolic Diseases, The First Affiliated Hospital of Hebei North University, Zhangjiakou, 075000, China. E-mail: zpanpan0903@sina.com*

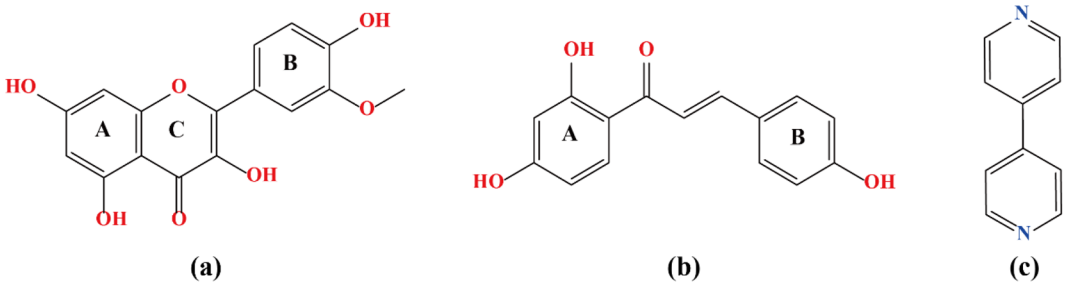

Fig. 1 Chemical structures of isorhamnetin (IRN) (a), isoliquiritigenin (ISL) (b) and 4,4′-bipyridine (4,4′-BPY) (c).

expression.[13,14] Similar to IRN, ISL is reported to induce tumor apoptosis, autophagy and angiogenesis through multiple signaling pathways such as PI3K/Akt, VEGF/VEGF2 and so on.[15,16] It is obvious that IRN and ISL possess significant potential for application in cancer treatment. Unfortunately, their low water solubility and poor bioavailability severely limit their new drug development and clinical application.

To address the challenges and difficulties of poor water solubility and low bioavailability of flavonoids and other natural products, a series of approaches have been taken into consideration, including solubilization, micronization, solid dispersions, nanotechnology and so on.[17,18] However, these approaches still have some shortcomings and limitations. For example, solubilization potentially has side effects on drug absorption and stability while improving solubility; micronization often suffers from poor flowability and susceptibility to electrostatic adhesion; solid dispersions exhibit drawbacks including high carrier material consumption, hygroscopicity and poor drug-carrier compatibility; and nanotechnology may face various challenges such as complex preparation processes, high technical difficulty, elevated costs and so on.[19–21] Compared with these technologies, cocrystal technology is considered as a simple, green and efficient strategy to address various dilemmas in the development of natural product-based drugs.[22] Without requiring further modification or carrier participation, cocrystal engineering spontaneously fabricates ordered supramolecular structures through non-covalent bonds such as hydrogen bonds, electrostatic interactions and π–π stacking;[23,24] cocrystal engineering offers the advantages of high drug loading capacity, simple preparation and environmental friendliness. Besides, cocrystal engineering can not only optimize compressibility, mechanical properties, stability, solubility, permeability and bioavailability but also reduce drug toxicity, improve drug therapeutic effects, and exploit pharmaceutical synergistic effects of individual components.[25–28]

Based on the multiple advantages of cocrystal technology, addressing the low water solubility and poor bioavailability of IRN and ISL with cocrystal engineering is brought to the forefront in this study. In order to prepare the cocrystals of IRN and ISL successfully, the selection of suitable coformers plays a significant role in the design and screening of cocrystals. Considering the structural characteristics and acid–base properties of IRN and ISL, the principle of cocrystal formation, the rule of ΔpK_a as well as the successful examples of flavonoid cocrystals from the CSD (Cambridge database) and relevant literature,[29–37] 4,4′-bipyridine (4,4′-BPY, Fig. 1c) caught our attention. The alkalinity and pyridine ring structure of 4,4′-BPY lay the groundwork for the formation of hydrogen bonding and π–π stacking in the cocrystals, which led us to believe that 4,4′-BPY is a fixed cocrystal coformer. Besides, 4,4′-BPY is an important intermediate applied in organic syntheses and the pharmaceutical industry.[29,38] Thus, 4,4′-BPY was chosen as the coformer of IRN and ISL in the cocrystal design.

In this study, the two crystal structures of IRN-4,4′-BPY (2 : 3) and ISL-4,4′-BPY (1 : 1) were first obtained and analyzed. Then, the preparation, characterization, structural analysis, stability, dissolution and anticancer activities of these two cocrystals were investigated to determine the influences on the physicochemical properties and pharmacological activities of IRN and ISL after their cocrystals are formed. During the course of the investigation, the differences between IRN-4,4′-BPY (2 : 3) and ISL-4,4′-BPY (1 : 1) in the aspects of structure and properties were compared and analyzed. According to the evaluation of these two cocrystals, it was found that the two obtained cocrystals exhibited satisfactory stabilities and significantly optimized the anticancer activities of IRN and ISL. As expected, the IRN-4, 4′-BPY (2 : 3) cocrystal improved the solubility and dissolution rate of IRN. Unexpectedly, the ISL-4,4′-BPY (1 : 1) cocrystal did not enhance the solubility and dissolution rate of ISL. Thus, with the help of cocrystal technology, two new cocrystals were prepared to improve the anticancer effects of IRN and ISL, which not only overcame the druggability difficulties in the development of IRN and ISL but also provided successful cases for the cocrystal study of flavonoids.

Experimental section

Materials

IRN (purity > 98%, MW = 316.26) was purchased from Chengdu Purui Technology Co., Ltd. (Sichuan, China), ISL (purity > 98%, MW = 256.25) was purchased from Nanjing Bingcheng Biotechnology Co., Ltd. (Jiangsu, China) and 4,4′-BPY (purity > 98%, MW = 156.18) was purchased from Aladdin Reagent Co., Ltd. (Shanghai, China). All the solvents used for crystallization were of analytical grade and purchased from Sinopharm Chemical Reagent Co., Ltd. (Beijing, China). The cancer cell line A549 was originally obtained from the Chinese Academy of Sciences Cell Bank (Shanghai, China), Dulbecco's modified

Eagle's medium (DMEM) was purchased from Gibco Life Technologies (Melbourne, Australia), fetal bovine serum (FBS) and cell counting kit-8 (CCK-8) were purchased from Boster Biological Technology Co., Ltd. (Wuhan, China), trypsin-0.02% EDTA (0.25%) and dimethyl sulphoxide (DMSO) were purchased from Beijing Solarbio Science & Technology Co., Ltd. (Beijing, China) and the mixture solution containing penicillin, streptomycin, and amphotericin B was purchased from Hebei Report Biotechnology Co., Ltd. (Hebei, China). All cell culture plastics were from Shijiazhuang Bende Biotechnology Co., Ltd (Hebei, China). Acetonitrile, methanol and acetic acid (HPLC grade) were obtained from Fisher Scientific (Shanghai, China).

Preparation of the IRN-4,4′-BPY (2 : 3) and ISL-4,4′-BPY (1 : 1) cocrystals

At a molar ratio of 2 : 3, 0.4 mmol of IRN (126.50 mg) and 0.6 mmol of 4,4′-BPY (93.71 mg) were accurately weighed and placed in a vial. Next, 12 mL of ethanol was added to the vial, and the mixture was stirred at a 300 rpm speed for 72 h under the condition of room temperature. Similarly, 0.5 mmol of ISL (128.13 mg) and 0.5 mmol of 4,4′-BPY (78.09 mg) were accurately weighed and placed in a vial at a molar ratio of 1 : 1. Then, 12 mL of ethanol was added to the vial, and the mixture was stirred at a 300 rpm speed for 72 h under the condition of room temperature. Finally, their suspensions were dried at 40 °C under reduced pressure for 72 h to get the powder samples of the IRN-4,4′-BPY and ISL-4,4′-BPY cocrystals.

Preparation of single crystals

With the help of evaporation crystallization, the single crystals of the IRN-4,4′-BPY (2 : 3) and ISL-4,4′-BPY (1 : 1) cocrystals were obtained. 0.1 mmol of IRN (31.63 mg) and 0.15 mmol of 4,4′-BPY (23.43 mg) were accurately weighed into a vial at a molar ratio of 2 : 3, 15 mL of ethanol was added and the mixture was stirred at 300 rpm for 72 h under room temperature. Then, 0.5 mL of *N*,*N*-dimethylformamide was added to the obtained suspension, and the mixture was heated at 60 °C in a water bath for 10 min to make it fully dissolved. The clear and transparent filtrates were obtained *via* filtering and evaporated at room temperature. After three weeks, some colorless block crystals were obtained. 0.2 mmol of ISL (51.25 mg) and 0.2 mmol of 4,4′-BPY (31.24 mg) were accurately weighed into a vial at a molar ratio of 1 : 1, 15 mL of ethanol was added and the mixture was stirred at 300 rpm for 72 h under room temperature. The solution was filtered to obtain clear and transparent filtrates, and the filtrates were evaporated at room temperature. After two weeks, some yellow block crystals were obtained.

Single-crystal X-ray diffraction (SCXRD)

At a temperature of 293 K, the SCXRD of IRN-4,4′-BPY (2 : 3) and ISL-4,4′-BPY (1 : 1) was performed on a Bruker APEX-II charge-coupled device (Bruker, Germany) with Cu-Kα radiation ($w\lambda$ = 1.54178 Å). The structures of the qualified single-crystal samples obtained in this study were resolved by the direct method and refined using the full-matrix least squares technique. With an isotropic displacement parameter, the non-hydrogen atoms were refined. For hydrogen atoms, they were placed at the calculated positions and refined with a riding model. Relying on the OLEX2 program, the obtained SCXRD data were processed and analyzed. Besides, molecular diagrams and various forces were depicted with the Mercury software (version 2025.3.1).

Powder X-ray diffraction (PXRD)

In this study, a series of PXRD experiments were performed on a MiniFlex600 diffractometer (Rigaku, Japan) with a Cu-Kα radiation source set at 40 kV and 15 mA. At a scan rate of 8° min^{-1}, the diffraction data were collected in the 2θ range of 3–40°. All the PXRD data were analyzed and processed using the Jade 6.0 software.

Infrared spectra (IR)

The infrared spectra of all experimental samples were recorded on a Nicolet iS5 FTIR spectrophotometer (Thermo Fisher Scientific, USA) with an attenuated total reflectance sampling accessory. The wavenumber ranged from 4000 to 550 cm^{-1} with 16 scans at a resolution of 4 cm^{-1}.

Thermal analysis

In this study, thermal analysis was performed on a Mettler Toledo DSC/DSC 1 equipment (Mettler Toledo, Switzerland) under a nitrogen gas flow of 50 mL min^{-1}. During the experiment, the samples to be tested were accurately weighed and put in hermetically sealed aluminum crucibles with a pinhole. At a constant rate of 10 °C min^{-1}, the samples were heated from 30 °C to a specified temperature, and their thermodynamic curves were recorded.

The TG analysis of the samples was performed on a Mettler Toledo DSC/TGA2+ equipment (Mettler Toledo, Switzerland) under a nitrogen gas flow of 50 mL min^{-1}. During the experiment, the accurately weighed samples in aluminum oxide crucibles were heated from 30 to 500 °C at a constant rate of 10 °C min^{-1}.

The obtained DSC and TG data were analyzed and processed with the STAR software V16.30 (Mettler Toledo, Switzerland).

Stability study

Placed in open containers, the stabilities of IRN-4,4′-BPY (2 : 3) and ISL-4,4′-BPY (1 : 1) were evaluated under three different conditions, including high temperature (60 ± 2 °C), high humidity (25 ± 2 °C, 90% ± 5%) and illumination (4500 ± 500 lx) for 5 days and 10 days. The phase changes were observed with PXRD to figure out whether the IRN-4,4′-BPY (2 : 3) and ISL-4,4′-BPY (1 : 1) cocrystals can remain stable under these three extreme conditions.

Powder dissolution *in vitro*

In order to remove the impact of sample particle size on the results of the experiments, all experimental samples were sieved through a 100-mesh sieve in advance. Using an RC-806 (Tianjin Tianda Tianfa Technology Co., Ltd, Tianjin, China), the

dissolution investigation of IRN, IRN-4,4′-BPY (2 : 3), ISL and ISL-4,4′-BPY (1 : 1) was performed. After each sampling, an equal volume of the blank dissolution medium was injected into the dissolution vessels to keep the total volume of the medium constant. Accurately weighed IRN (60.0 mg), the IRN-4,4′-BPY (2 : 3) cocrystal (104.4 mg, which is equivalent to 60.0 mg ACT), ISL (60.0 mg), and the ISL-4,4′-BPY (1 : 1) cocrystal (96.6 mg, which is equivalent to 60.0 mg ISL) were added to dissolution vessels containing 900 mL media, including 0.1 M hydrochloric acid aqueous solution (pH = 1.2), acetate buffer (pH = 4.5), phosphate buffer (pH = 6.8) and pure water (pH = 7.0). Samples were stirred at 100 rpm in different dissolution vessels, which were bathed in 37 °C water. 1 mL of each sample was collected at 0, 5, 15, 30, 60, 120, 240, 360 and 480 min. Then, the concentration of IRN or ISL in these samples was determined by HPLC. The liquid-phase conditions were as follows: Welch Ultimate XB-C18 (250 mm × 4.6 mm, 5 μm); mobile phase, methanol–0.2% acetic acid water (75 : 25, v/v) for IRN and methanol–0.1% acetic acid water (80 : 20, v/v) for ISL; detection wavelength, 370 nm for IRN and 365 nm for ISL; flow rate, 1.0 mL min; column temperature, 30 °C; and injection volume, 10 μL.

Cell culture and treatment and anticancer activity assessment using CCK-8 assay

The A549 cells were cultured with DMEM supplemented with 10% FBS as well as 1% mixture solution containing penicillin, streptomycin, and amphotericin B and maintained in exponential growth at 37 °C in a humidified atmosphere under 5% CO_2. Cells were sub-cultured every third day (1 : 3) using trypsinization (0.25%, w/v, trypsin in D-Hanks sodium with 0.2% EDTA-2Na) and used within 20 passages of the initial stock culture.

Log-phase cells with the density of 5×10^4 cells per mL were randomly assigned into two parts, namely, part A and part B. The cells in part A were randomly assigned into four groups (n = 6 per group) as described below. Blank control group: cells were incubated with blank medium for 24 h and exposed to the replaced blank medium containing 10 μL of 0.1% DMSO for another 24 h. IRN group: cells were incubated with blank medium for 24 h and exposed to the replaced blank medium containing 10 μL of IRN (2.0 μg mL^{-1}) for another 24 h. IRN-4,4′-BPY (2 : 3) cocrystal group: cells were incubated with blank medium for 24 h and exposed to the replaced blank medium containing 10 μL of the IRN-4,4′-BPY (2 : 3) cocrystal (3.48 μg mL^{-1}, which is equivalent to 2.0 μg mL^{-1} IRN) for another 24 h. The physical mixture of IRN and 4,4′-BPY group: cells were incubated with blank medium for 24 h and exposed to the replaced blank medium containing 10 μL of the physical mixture (3.48 μg mL^{-1}, which is equivalent to 2.0 μg mL^{-1} IRN) for another 24 h. The cells in part B were randomly assigned into four groups (n = 6 per group) as described below. Blank control group: cells were incubated with blank medium for 24 h and exposed to the replaced blank medium containing 10 μL of 0.1% DMSO for another 24 h. ISL group: cells were incubated with blank medium for 24 h and exposed to the replaced blank medium containing 10 μL of ISL (10.0 μg mL^{-1}) for another 24 h. ISL-4,4′-BPY (1 : 1) cocrystal group: cells were incubated with blank medium for 24 h and exposed to the replaced blank medium containing 10 μL of the ISL-4,4′-BPY (1 : 1) cocrystal (16.09 μg mL^{-1}, which is equivalent to 10.0 μg mL^{-1} ISL) for another 24 h. The physical mixture of ISL and 4,4′-BPY group: cells were incubated with blank medium for 24 h and exposed to the replaced blank medium containing 10 μL of the physical mixture (16.09 μg mL^{-1}, which is equivalent to 10.0 μg mL^{-1} ISL) for another 24 h. IRN, IRN-4,4′-BPY (2 : 3) and the physical mixture of IRN and 4,4′-BPY at an equimolar ratio were dissolved in 0.1% DMSO, and the same was done for ISL, ISL-4,4′-BPY (1 : 1) and the physical mixture of ISL and 4,4′-BPY.

After 24 h of incubation, 10 μL of CCK-8 was added to each well and incubated at 37 °C for 1 h. Then, the absorbance of each well at 450 nm was detected with a microplate reader, and every absorbance value was measured in triplicate. The % cell inhibition was determined using the following formula.[39]

$$\%\ \text{Cell inhibition} = 100 \times \left(1 - \frac{\text{absorbance of the sample}}{\text{absorbance of the control}}\right)$$

Using SPSS 26.0, differences between different groups were analyzed by the one-way analysis of variance (ANOVA) followed by Tukey's tests. The processed data were expressed as mean ± standard deviation (SD). Besides, statistical significance was considered at $P < 0.05$.

Results and discussion

SCXRD analysis

As humanity's eyes into the microscopic world, SCXRD technology can transform abstract atomic arrangements into visualizable three-dimensional models.[40] With the advantages such as high precision, comprehensive information coverage, authoritative results and non-destructive operation, this technology is considered an indispensable core analytical tool in modern chemistry, materials science, structural biology, pharmaceutical research and various related fields.[41] Based on the results of the SCXRD analysis, a series of information on the two cocrystals, including crystal data, structure refinement parameters and hydrogen bonds, were obtained and summarized in Tables 1 and 2. At the same time, the crystal structure diagrams of the two cocrystals, including the asymmetric units and two-dimensional layered structures, are depicted in Fig. 2. As presented in Table 1, the crystal structure of IRN-4,4′-BPY (2 : 3) belongs to the $P\bar{1}$ space group of the triclinic crystal system with $Z = 2$, and ISL-4,4′-BPY (1 : 1) belongs to the $P2_1/c$ space group of the monoclinic crystal system with $Z = 4$.

In Fig. 2a-1, there are two IRN and three 4,4′-BPY in the asymmetric unit, whose molar ratio (2 : 3) is different from the majority of reported cocrystals composed of flavonoids and 4,4′-BPY.[29–36] Combining this with the information of hydrogen bonds depicted in Table 2, it is found that two IRN interact with three 4,4′-BPY to generate a five-element structure through the hydrogen bonds of O5–H5···N1L (2.695 Å) and O6–H6···N3L (2.795 Å) in the asymmetric unit. From the view of the "b" axis, adjacent five-element structures are linked to form a chain

Table 1 Crystal data and structure refinement parameters of the IRN-4,4′-BPY (2 : 3) and ISL-4,4′-BPY (1 : 1) cocrystals

Parameters	IRN-4,4′-BPY (2 : 3)	ISL-4,4′-BPY (1 : 1)
Empirical formula	$C_{31}H_{24}N_3O_7$	$C_{25}H_{20}N_2O_4$
Formula weight	550.53	412.43
Crystal size/mm	0.14 × 0.16 × 0.19	0.15 × 0.20 × 0.21
Description	Block	Block
Crystal system	Triclinic	Monoclinic
Space group	$P\bar{1}$	$P2_1/c$
a (Å)	9.415(1)	16.997(1)
b (Å)	11.187(1)	9.484(1)
c (Å)	13.236(1)	12.886(1)
α (°)	80.21(1)	90.00
β (°)	89.11(1)	97.23(1)
γ (°)	77.04(1)	90.00
Volume (Å^3)	1338.4(2)	2060.7(1)
Z	2	4
Completeness	99.8%	98.8%
Density (g cm^{-3})	1.366	1.329
Reflections with $I > 2\sigma$ (I)	3240	2815
R Index ($I > 2\sigma I$)	$R_1 = 0.059$ $wR_2 = 0.157$	$R_1 = 0.057$ $wR_2 = 0.156$
Goodness-of-fit on F^2	1.022	1.033
CCDC deposition number	2526401	2526402

Table 2 Hydrogen bonds of the IRN-4,4′-BPY (2 : 3) and ISL-4,4′-BPY (1 : 1) cocrystals

Crystal name	D–H⋯A	d(D⋯A) (Å)	∠(DHA) (deg)	Symmetry code
IRN-4,4′-BPY	O2–H2⋯O3	2.715	113.63	—
(2 : 3)	O2–H2⋯O3	2.688	146.21	[−x, −y, −z + 1]
	O4–H4⋯O3	2.641	145.99	—
	O5–H5⋯N1L	2.695	173.43	—
	O6–H6⋯N3L	2.795	174.31	—
ISL-4,4′-BPY	O1–H1⋯O3	2.532	147.42	—
(1 : 1)	O2–H2⋯N2L	2.700	163.34	[x + 1, −y + 3/2, z + 3/2]
	O4–H4⋯N1L	2.684	149.90	—

structure along the direction of "a", which depends on the hydrogen bond O5–H5⋯O6 (2.835 Å). Along the direction of "c", the adjacent chains are further connected to generate a neat laminar structure through O2–H2⋯O3 (2.688 Å) (Fig. 2a-2). Different from the IRN-4,4′-BPY (2 : 3) cocrystal, there is one ISL and one 4,4′-BPY in the asymmetric unit of the ISL-4,4′-BPY (1 : 1) cocrystal (Fig. 2b-1). As illustrated in Fig. 2b-2, ISL and 4, 4′-BPY are linked in a head-to-tail sequence to form a chain structure through the hydrogen bonds including O4–H4⋯N1L (2.684 Å) and O2–H2⋯N2L (2.700 Å). From the view of the "c" axis, this chain structure is along the direction of "b". Based on this chain structure, the adjacent chains are further connected to generate a neat laminar structure along the direction of "a", which relies on the dislocated parallel π–π stacking between the two pyridine rings of 4,4′-BPY and the A ring as well as the B ring of ISL. By analyzing the crystal structures of IRN-4,4′-BPY (2 : 3) and ISL-4,4′-BPY (1 : 1), significant differences are found among these two cocrystals. These differences mainly exist in aspects such as the type of space group and crystal system, lattice arrangement, and the forces and hydrogen bonds involved in the formation of the two cocrystals, which are closely related to the structural differences between IRN and ISL as well as the spatial site resistance encountered in the lattice arrangement.

PXRD analysis

It is well known to us that each material possesses its own unique PXRD pattern, and PXRD technology serves as a fingerprint for precisely identifying the phase states of different substances. As the most fundamental and widely applied field of PXRD technology, phase identification using PXRD plays significant role in various areas such as materials science, chemical engineering and pharmaceuticals.[42] In this study, the phase transformations after generating cocrystals were identified and monitored with PXRD. As depicted in Fig. 3a, IRN exhibits its unique characteristic crystalline peaks at 2θ values of 9.19°, 9.88°, 10.45°, 13.47°, 17.43°, 18.43°, 20.88°, 23.84°, 25.65°, 27.19°, 27.66° and 37.55°, and 4,4′-BPY exhibits its unique characteristic crystalline peaks at 2θ values of 12.48°, 13.24°, 17.69°, 19.55°, 23.03°, 25.79°, 27.82° and 30.45°. Distinct from the PXRD patterns of IRN and 4,4′-BPY, a series of new characteristic crystalline peaks emerged at 2θ values of 6.66°, 9.59°, 11.07°, 13.94°, 16.75°, 20.84°, 24.24° and 28.58° in the powder XRD pattern of IRN-4,4′-BPY (2 : 3). Fig. 3b displays that ISL exhibits its unique characteristic crystalline peaks at 2θ values of 7.14°, 14.33°, 16.31°, 18.84°, 24.42°, 25.78°, 28.67° and 33.18°. Compared with the powder XRD patterns of ISL and 4,4′-BPY, there were obvious differences in the powder XRD pattern

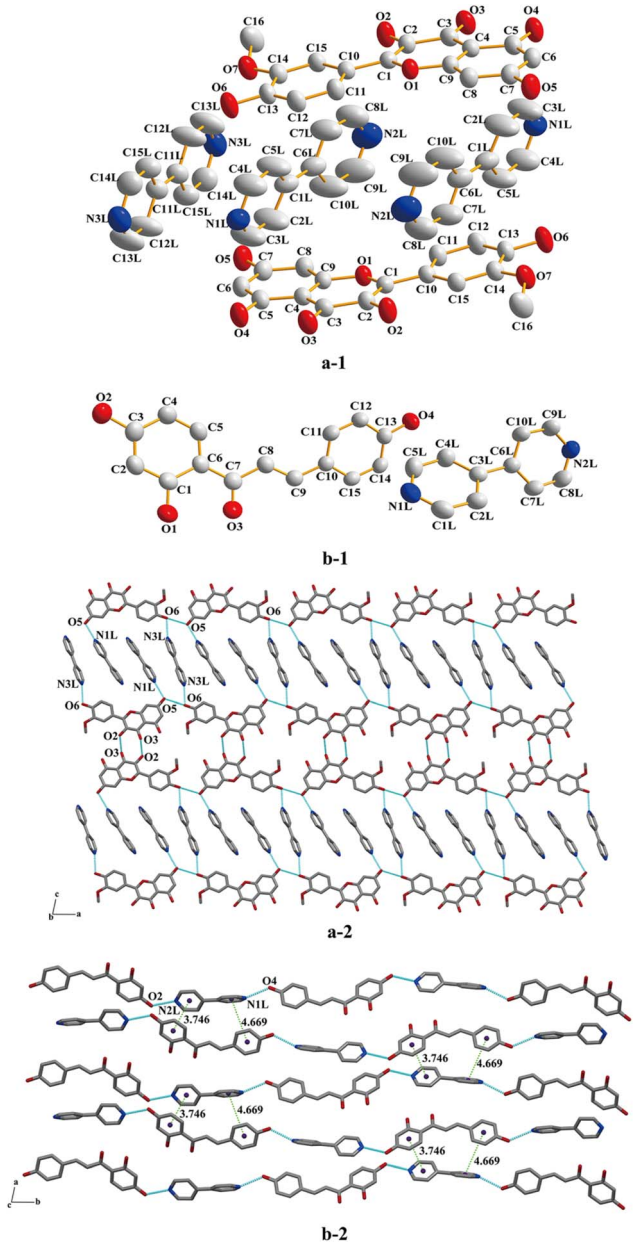

Fig. 2 Crystal structures of the IRN-4,4′-BPY (2 : 3) and ISL-4,4′-BPY (1 : 1) cocrystals: (a-1) ellipsoid plot of IRN-4,4′-BPY (2 : 3), (a-2) 2D layer structure of IRN-4,4′-BPY (2 : 3) viewed from the *b* axis, (b-1) ellipsoid plot of ISL-4,4′-BPY (1 : 1), and (b-2) 2D layer structure of ISL-4,4′-BPY (1 : 1) viewed from the *c* axis.

of ISL-4,4′-BPY (1 : 1), whose new characteristic crystalline peaks appeared at 2θ values of 12.32°, 13.84°, 15.39°, 18.33°, 22.19°, 23.75°, 24.82°, 27.30° and 32.58°. Based on the results of PXRD, the fact that new crystalline phases were generated was proved by the evidence that the characteristic peaks of IRN, ISL and 4,4′-BPY disappeared and the new peaks of these two cocrystals emerged. The good match between the simulated powder patterns calculated from the SXRD data of the two cocrystals and their experimental PXRD patterns confirmed the formation of these two cocrystals.

IR analysis

As a powerful tool to characterize cocrystals, IR can contribute to the identification of hydrogen bond types and confirmation of cocrystal formation by detecting spectral shifts aroused by intermolecular interactions. As illustrated in Fig. 4a, the free O–H stretching absorption peak was observed at 3213 cm^{-1} and the C–O stretching absorption peak was positioned at 1032 cm^{-1} in the IR spectrum of IRN. As illustrated in Fig. 4b, the free O–H stretching absorption peak was observed at 3378 cm^{-1} and the C–O stretching absorption peak was positioned at 1031 cm^{-1} in the IR spectrum of ISL. Besides, the C=N stretching absorption peak in the IR spectrum of 4,4′-BPY was positioned at 1586 cm^{-1}. In the IR spectrum of the IRN-4,4′-BPY (2 : 3) cocrystal (Fig. 4a), the O–H stretching absorption peak appeared at 3057 cm^{-1} and the C–O stretching absorption peak was observed at 1030 cm^{-1}, which were respectively attributed to the red shift from the ν_{O-H} at 3213 cm^{-1} and ν_{C-O} at 1032 cm^{-1} in the IR spectrum of IRN. The C=N stretching absorption peak in the IR spectrum of the IRN-4,4′-BPY (2 : 3) cocrystal emerged at 1558 cm^{-1}, which might be due to the red shift from the $\nu_{C=N}$ at 1586 cm^{-1} in the 4,4′-BPY IR spectrum. In the IR spectrum of the ISL-4,4′-BPY (1 : 1) cocrystal (Fig. 4b), the O–H stretching absorption peak appeared at 3062 cm^{-1} and the C–O stretching absorption peak was observed at 1028 cm^{-1}, which were respectively attributed to red shift from the ν_{O-H} at 3378 cm^{-1} and ν_{C-O} at 1031 cm^{-1} in the IR spectrum of ISL. The C=N stretching absorption peak in the IR spectrum of the IRN-4,4′-BPY (2 : 3) cocrystal emerged at 1556 cm^{-1}, which might be due to the red shift from the $\nu_{C=N}$ at 1586 cm^{-1} in the 4,4′-BPY IR spectrum. Based on the results of IR, hydrogen bonds were further confirmed to participate in the formation of the IRN-4,4′-BPY (2 : 3) and ISL-4,4′-BPY (1 : 1) cocrystals.

Thermal analysis

Just like a high-precision calorimetric microscope, DSC can detect and quantify heat absorption and release events during temperature changes, which can not only determine the purity of the compound but also monitor its phase transition.[43] It is presented in Fig. 5a that the IRN-4,4′-BPY (2 : 3) cocrystal exhibits a sharp endothermic peak at 216.13 °C, which is significantly distinct from the endothermic peaks of IRN (321.17 °C) and 4,4′-BPY (114.11 °C). Similarly, Fig. 5b shows that the ISL-4,4′-BPY (1 : 1) cocrystal exhibits a sharp endothermic peak at 207.44 °C, which is different from the endothermic peaks of ISL (202.48 °C) and 4,4′-BPY (114.11 °C). The results of DSC demonstrated that there were two new solid phases generated, and these newly formed solid phases exhibited high purity, which further confirmed the formation of the IRN-4,4′-BPY (2 : 3) and ISL-4,4′-BPY (1 : 1) cocrystals.

As a thermal analysis technology to measure the mass change of a sample with temperature, TG analysis is usually adopted to monitor and quantify the mass changes of substances caused by volatilization, decomposition and other by-reactions during heating.[44] During heating from 30 to 500 °C, there were two weight loss steps in the TG curve of IRN-4,4′-BPY (2 : 3) cocrystal (Fig. 6a). The first weight loss was 25.9% from

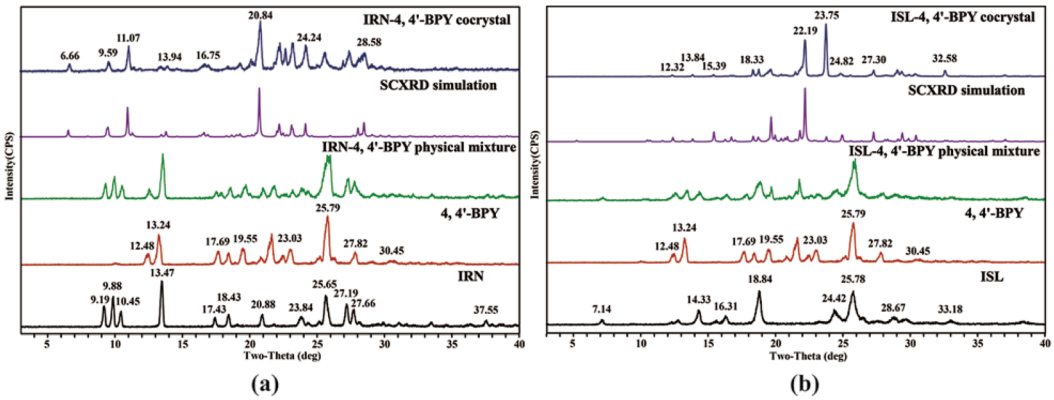

Fig. 3 PXRD patterns of IRN-4,4′-BPY (2 : 3) (a) and ISL-4,4′-BPY (1 : 1) (b).

135 to 215 °C, and the second weight loss was 59.7% from 215 to 500 °C. Different from the IRN-4,4′-BPY (2 : 3) cocrystal, the ISL-4,4′-BPY (1 : 1) cocrystal showed only one weight loss step in its TG curve, and its weight loss was 61.1% from 170 to 500 °C (Fig. 6b). Based on the TG analysis, there were no solvent or water weight loss steps to be found, which indicated that these two new cocrystals did not contain any solvents or water.

Stability study

Stability is an essential determinant of pharmaceutical druggability; it determines the shelf life of pharmaceuticals and influences their storage and transportation.[45,46] For oral solid drugs, stability issues occur along with changes in their physical phase state. Such changes will result in different alterations in peak positions, intensities, shapes, and topological peak shapes in the PXRD pattern. With the help of PXRD analysis, the stability of the IRN-4,4′-BPY (2 : 3) and ISL-4,4′-BPY (1 : 1) cocrystals was evaluated under high temperature, high humidity and illuminated environments in this study. The PXRD patterns of these two cocrystals at 0, 5 and 10 days were compared to observe whether their PXRD patterns changed in the aspects of peak positions, intensities, shapes and topological peak configurations. Under the three conditions, on the 5th and 10th day, there were almost no significant changes in their PXRD patterns (Fig. 7), which suggested that the IRN-4,4′-BPY (2 : 3) and ISL-4,4′-BPY (1 : 1) cocrystals could remain stable in the same crystal form under high temperature, high humidity and illuminated conditions.

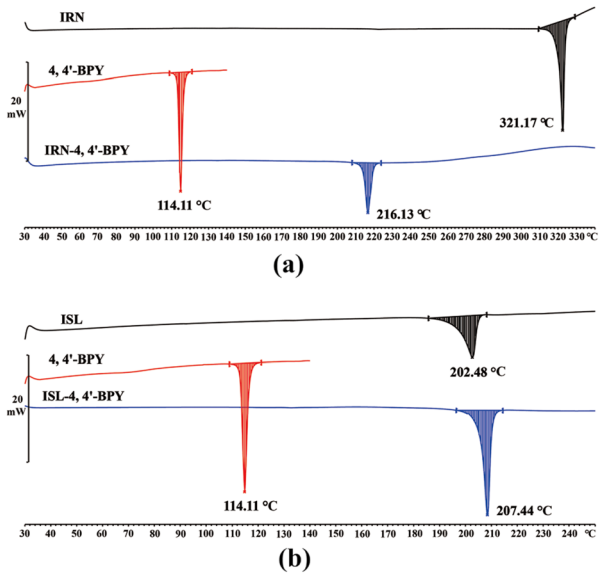

Fig. 5 DSC plots of IRN-4,4′-BPY (2 : 3) (a) and ISL-4,4′-BPY (1 : 1) (b).

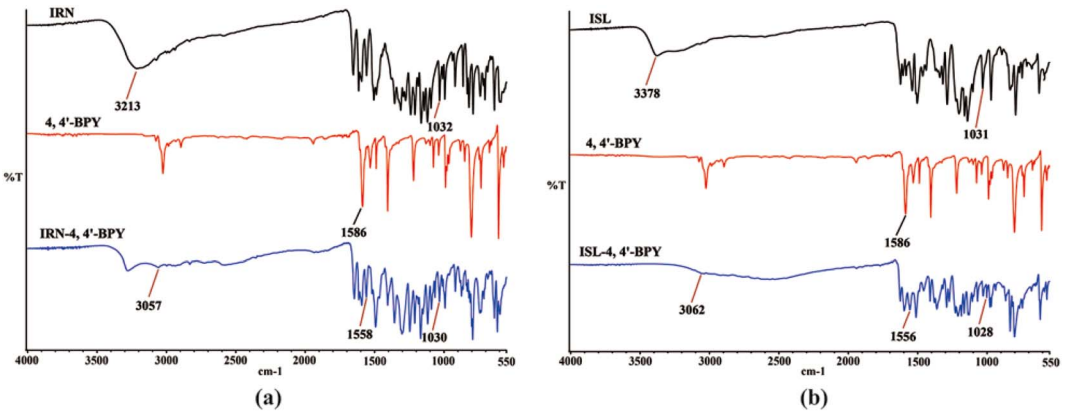

Fig. 4 IR spectra of IRN-4,4′-BPY (2 : 3) (a) and ISL-4,4′-BPY (1 : 1) (b).

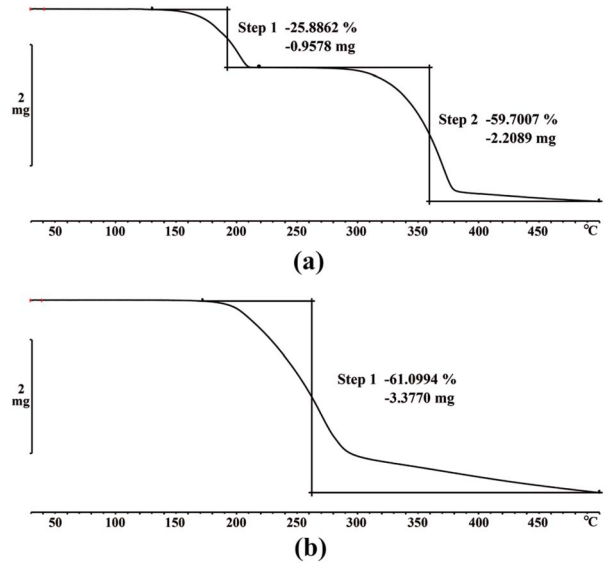

Fig. 6 TG plots of IRN-4,4′-BPY (2 : 3) (a) and ISL-4,4′-BPY (1 : 1) (b).

Powder dissolution *in vitro*

For poorly soluble compounds, the elevation in solubility and dissolution rate is crucial for their bioavailability. In the case of pure IRN, the maximum concentrations after 8 h were 0.208 ± 0.033, 0.115 ± 0.015, 0.109 ± 0.018 and 0.105 ± 0.009 μg mL^{-1} in four different mediums (pH 1.2, pH 4.5, pH 6.8 and pH 7.0), and the dissolution rates after 1 h were 0.103 ± 0.006, 0.039 ± 0.004, 0.042 ± 0.005 and 0.035 ± 0.004 μg mL^{-1} h^{-1}, respectively, in these mediums. Correspondingly, the maximum concentrations of IRN released from the IRN-4,4′-BPY (2 : 3) cocrystal after 8 h were 1.521 ± 0.027, 0.846 ± 0.068, 0.432 ± 0.026 and 0.599 ± 0.114 μg mL^{-1} in the four different mediums, and the dissolution rates after 1 h were 1.159 ± 0.098, 0.255 ± 0.019, 0.323 ± 0.023 and 0.327 ± 0.014 μg mL^{-1} h^{-1}, respectively, in these mediums (Fig. 8a). Compared with the parent drug, the maximum concentrations of IRN released from the cocrystal after 8 h were 7.3-, 7.4-, 4.0- and 5.3-fold that of IRN in the four different mediums, and the dissolution rates of IRN released from the cocrystal after 1 h were 11.3-, 6.5-, 7.7- and 9.3-fold that of IRN in these mediums, respectively. According to the results listed above, it could be confirmed that the formation of the IRN-4,4′-BPY (2 : 3) cocrystal achieved a significant boost in both the dissolution amount and rate of IRN, which might be beneficial to optimize the bioavailability and anticancer efficacy of IRN.

In the case of pure ISL, the maximum concentrations after 8 h were 25.68 ± 0.88, 28.68 ± 1.49, 31.98 ± 1.15 and 26.96 ± 2.37 μg mL^{-1} in the four different mediums (pH 1.2, pH 4.5, pH 6.8 and pH 7.0), and the dissolution rates after 1 h were respectively 21.33 ± 0.36, 21.55 ± 6.18, 25.05 ± 6.42 and 21.54 ± 3.75 μg mL^{-1} h^{-1} in these mediums. Correspondingly, the maximum concentrations of ISL released from the ISL-4,4′-BPY (1 : 1) cocrystal after 8 h were 21.50 ± 0.23, 25.30 ± 0.59, 17.57 ± 0.76 and 17.08 ± 2.54 μg mL^{-1} in these mediums, and the dissolution rates after 1 h were respectively 13.29 ± 0.57, 20.44 ± 0.30, 14.12 ± 3.15 and 15.28 ± 0.31 μg mL^{-1} h^{-1} in these mediums (Fig. 8b). Disappointingly, the formation of ISL-4,4′-BPY (1 : 1) cocrystal did not achieve satisfactory solubility or dissolution rate, which suggested that not all cocrystals could improve the solubility of poorly soluble drugs.

Anticancer activity evaluation on the A549 cell line

The anticancer activity of the IRN-4,4′-BPY (2 : 3) and ISL-4,4′-BPY (1 : 1) cocrystals was evaluated on a human lung cancer cell line (A549) using CCK-8 assays. As illustrated in Fig. 9, the A549 cell inhibition rates when treated with IRN, the IRN-4,4′-BPY (2 : 3) cocrystal and the physical mixture of IRN and 4,4′-BPY were 14.1% ± 5.4%, 40.7% ± 6.7% and 25.5% ± 3.5%, respectively. Compared with those of the pure IRN and physical mixture, the A549 cell inhibition rate of the IRN-4,4′-BPY (2 : 3)

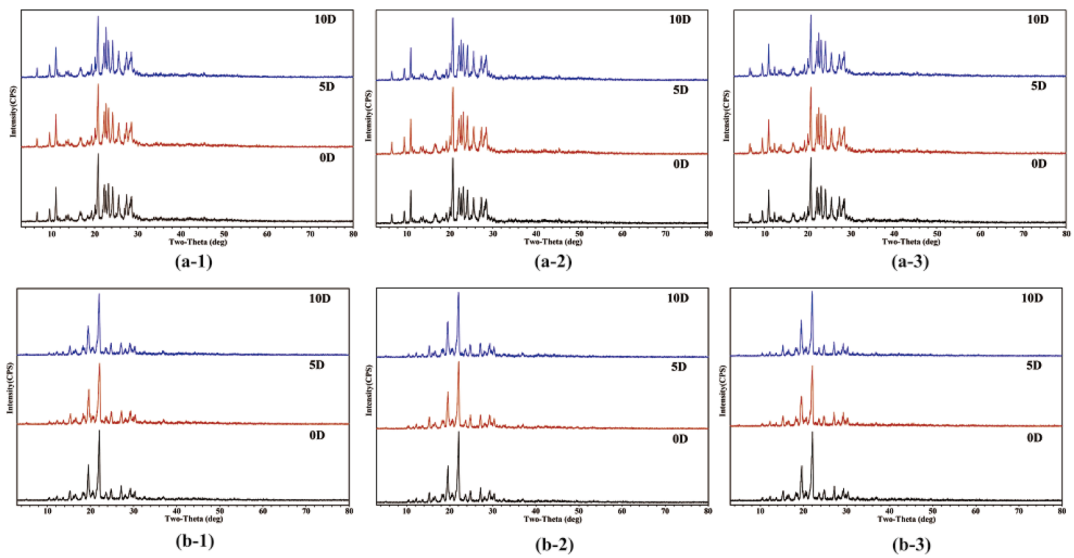

Fig. 7 Stability evaluations of IRN-4,4′-BPY (2 : 3) (a) and ISL-4,4′-BPY (1 : 1) (b) by PXRD analysis. (1: under illuminated environments, 2: under high temperature and 3: under high humidity).

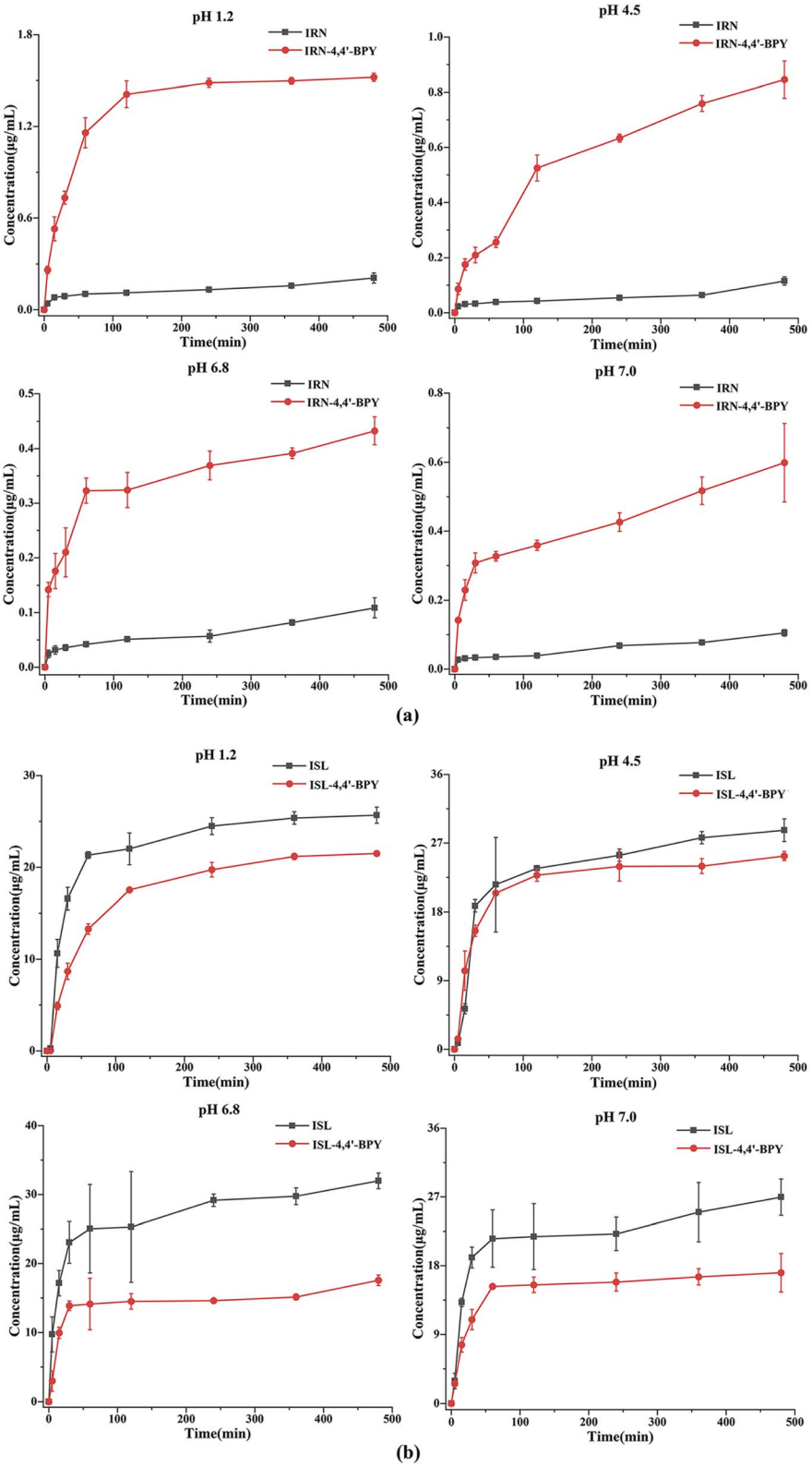

Fig. 8 Powder dissolution curves of pure IRN and the IRN-4,4′-BPY (2 : 3) cocrystal (a) as well as pure ISL and the ISL-4,4′-BPY (1 : 1) cocrystal (b) in four different media including pH 1.2, pH 4.5, pH 6.8 and pH 7.0 (There were $n = 3$ samples per group).

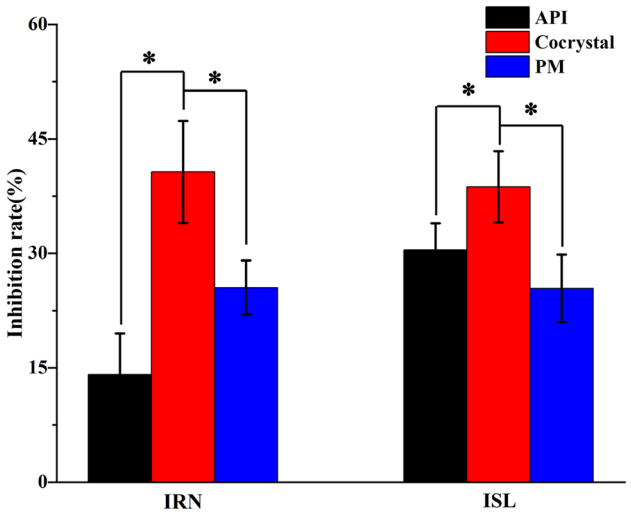

Fig. 9 Inhibition rates of two APIs (IRN and ISL), two cocrystals (the IRN-4,4′-BPY (2 : 3) and ISL-4,4′-BPY (1 : 1) cocrystals) and their physical mixtures (PMs) on the A549 lung cancer cells. (For the differences in the cell inhibition rate (%) of cocrystals *vs.* APIs and cocrystals *vs.* the physical mixtures, "*" represents "$P < 0.01$") (There were $n = 6$ cell samples per group).

cocrystal achieved a remarkable improvement ($P < 0.01$), which demonstrated that the formation of the IRN-4,4′-BPY (2 : 3) cocrystal significantly optimized the anticancer efficacy of IRN. For the other cocrystal, the A549 cell inhibition rates incubated with ISL, the ISL-4,4′-BPY (1 : 1) cocrystal and the physical mixture of ISL and 4,4′-BPY were 30.4% ± 3.5%, 38.7% ± 4.7% and 25.4% ± 4.4%, respectively. Compared with those of the pure ISL and physical mixture, the A549 cell inhibition rate of the ISL-4,4′-BPY (1 : 1) cocrystal realized a slight increase with a statistically significant difference ($P < 0.01$). In terms of the degree of enhancement in anticancer activity against A549 cells, the IRN-4,4′-BPY (2 : 3) cocrystal exhibited distinct advantages compared to the ISL-4,4′-BPY (1 : 1) cocrystal, which might have a tight correlation with the great potential of the IRN-4,4′-BPY (2 : 3) cocrystal in improving the solubility and dissolution rate of IRN. Although the ISL-4,4′-BPY (1 : 1) cocrystal did not reach the goal of enhancing the solubility of ISL, its anticancer activity was slightly increased, which explained that the ISL-4,4′-BPY (1 : 1) cocrystal might improve the permeability of ISL.

Conclusion

Different from conventional formulation approaches, such as liposomes, inclusion complexes, solid dispersions, micelles, nanoparticles and so on, a new and efficient method based on crystal engineering and supramolecular chemistry was adopted to optimize the solubilities and anticancer activities of IRN and ISL through a scientific cocrystal design, which not only avoided the involvement of carriers and excipients but also achieved a high drug loading capacity. In this study, two crystal structures consisting of the IRN-4,4′-BPY (2 : 3) and ISL-4,4′-BPY (1 : 1) cocrystals were obtained with evaporation crystallization, which were subjected to authoritative characterization and subsequent structural analysis. Combining various analytical technologies, including PXRD, IR, DSC and TG, the two newly prepared cocrystals were characterised and confirmed. From the structural analysis results, there were significant differences in the space group and crystal system, lattice arrangement and the forces and hydrogen bonds involved in the IRN-4,4′-BPY (2 : 3) and ISL-4,4′-BPY (1 : 1) cocrystals. At the same time, the phase transitions and thermodynamic properties of these two cocrystals were investigated with the help of PXRD, DSC and TG. A series of evaluations on the stability, dissolution and anticancer activity demonstrated that the IRN-4,4′-BPY (2 : 3) and ISL-4,4′-BPY (1 : 1) cocrystals could remain stable under three extreme conditions and realized significant elevation in their anticancer activities. To address the limitations of IRN and ISL in drug development and realize their improved anticancer activities, a rigorous and innovative attempt was launched. Without altering the original structure of IRN and ISL, this attempt not only merely validated the huge potential for the optimization of the pharmaceutical properties of IRN and ISL but also pioneered a new track to promote the development of highly effective, low-toxicity anticancer drugs.

Author contributions

Conceptualization, Zhipeng Wang, Panpan Zhao and Zhigang Wu; data curation, Zhipeng Wang, Yu Liu, Jian Lei and Ting Li; formal analysis, Aiyu Zhong, Junxiao Lv and Zihan Zhu; funding acquisition, Zhipeng Wang and Panpan Zhao; investigation, Yu Liu, Zhipeng Wang, Jian Lei and Ting Li; project administration, Zhipeng Wang, Zhigang Wu and Panpan Zhao; supervision, Zhigang Wu and Panpan Zhao; writing – original draft, Yu Liu and Zhipeng Wang; writing – review & editing, Zhipeng Wang, Zhigang Wu and Panpan Zhao.

Conflicts of interest

The authors declare that there are no competing interests in this study.

Data availability

The data of the compounds are available from the authors. Crystallographic data for the isorhamnetin-4,4′-bipyridine and isoliquiritigenin-4,4′-bipyridine cocrystals have been deposited at the CCDC under no. 2526401 and no. 2526402, which can be obtained from https://www.ccdc.cam.ac.uk/structures/.

CCDC 2526401 and 2526402 contain the supplementary crystallographic data for this paper.[47a,b]

Acknowledgements

The authors acknowledge the Hebei Provincial Basic Scientific Research Project (JYT2025002), the S&T Program of Zhangjiakou (2511022A) and the PhD Start-Up Fund of Hebei North University (BSJJ202533) for financing this work.

References

1 T. Zhang, F. Ding, Y. Yang, G. Zhao, C. Zhang, R. Wang and X. Huang, *Biosensors*, 2022, **12**(7), 485.
2 P. Brennan and G. Davey-Smith, *J. Natl. Cancer Inst.*, 2022, **114**(3), 353–360.
3 J. Zhao, R. Ren, N. M. Beeraka, M. Pa, N. Xue, P. Lu, W. Bai, Z. Mao, H. V. Pr, K. V. Bulygin, V. N. Nikolenko, R. Fan and J. Liu, *Front. Oncol.*, 2024, **14**, 1398679.
4 Z. Wang, Y. Tian, H. Zhang, Y. Qin, D. Li, L. Gan and F. Wu, *Int. J. Nanomed.*, 2016, **11**, 6485–6497.
5 T. Al-Warhi, A. M. El Kerdawy, M. A. Said, A. Albohy, Z. M. Elsayed, N. Aljaeed, E. B. Elkaeed, W. M. Eldehna, H. A. Abdel-Aziz and M. A. Abdelmoaz, *Drug Des. Dev. Ther.*, 2022, **16**, 1457–1471.
6 A. Aydin and Ş. A. Korkmaz, *Iran. J. Pharm. Res.*, 2019, **18**(4), 2011–2027.
7 S. T. Asma, U. Acaroz, K. Imre, A. Morar, S. R. A. Shah, S. Z. Hussain, D. Arslan-Acaroz, H. Demirbas, Z. Hajrulai-Musliu, F. R. Istanbullugil, A. Soleimanzadeh, D. Morozov, K. Zhu, V. Herman, A. Ayad, C. Athanassiou and S. Ince, *Cancers*, 2022, **14**(24), 6203.
8 A. Naeem, P. Hu, M. Yang, J. Zhang, Y. Liu, W. Zhu and Q. Zheng, *Molecules*, 2022, **27**(23), 8367.
9 Y. Luo, Y. Jian, Y. Liu, S. Jiang, D. Muhammad and W. Wang, *Molecules*, 2022, **27**(3), 719.
10 P. Karak, *Int. J. Pharm. Sci. Res.*, 2019, **10**(4), 1567–1574.
11 A. M. Malla, B. A. Dar, A. B. Isaev, Y. Lone and M. R. Banday, *Mini-Rev. Med. Chem.*, 2023, **23**(7), 772–786.
12 S. Tang, B. Wang, X. Liu, W. Xi, Y. Yue, X. Tan, J. Bai and L. Huang, *Food Front.*, 2025, **6**(1), 218–247.
13 P. Biswas, M. A. Kaium, M. M. I. Tareq, S. J. Tauhida, M. R. Hossain, L. S. Siam, A. Parvez, S. Bibi, M. H. Hasan, M. M. Rahman, D. Hosen, M. A. I. Siddiquee, N. Ahmed, M. Sohel, S. A. Azad, A. H. Alhadrami, M. Kamel, M. K. Alamoudi, M. N. Hasan and M. M. Abdel-Daim, *Biomed. Pharmacother.*, 2024, **176**, 116860.
14 M. Ganbold, P. Louphrasitthiphol, T. Miyamoto, Y. Miyazaki, T. Oda, K. Tominaga and H. Isoda, *Biomed. Pharmacother.*, 2025, **185**, 117954.
15 K. L. Wang, Y. C. Yu and S. M. Hsia, *Cancers*, 2021, **13**(1), 115.
16 T. T. Zhao, Y. Q. Xu, H. M. Hu, H. B. Gong and H. L. Zhu, *Curr. Med. Chem.*, 2019, **26**(37), 6786–6796.
17 S. Jain, N. Patel and S. Lin, *Drug Dev. Ind. Pharm.*, 2015, **41**(6), 875–887.
18 L. Kumari, Y. Choudhari, P. Patel, G. D. Gupta, D. Singh, J. M. Rosenholm, K. K. Bansal and B. D. Kurmi, *Life*, 2023, **13**(5), 1099.
19 P. Chakravarty, A. Famili, K. Nagapudi and M. A. Al-Sayah, *Pharmaceutics*, 2019, **11**(12), 629.
20 R. Malkawi, W. I. Malkawi, Y. Al-Mahmoud, J. Tawalbeh and S. Mutalik, *Adv. Pharmacol. Pharm. Sci.*, 2022, **2022**, 1–17.
21 M. Ignatova, D. Paneva, S. Kyuchyuk, N. Manolova, I. Rashkov, M. Mourdjeva and N. Markova, *Polymers*, 2025, **17**(19), 2657.
22 Z. Wang, Y. Xie, M. Yu, S. Yang, Y. Lu and G. Du, *AAPS PharmSciTech*, 2022, **23**(8), 303.
23 W. Cai, D. Xu, L. Qian, J. Wei, C. Xiao, L. Qian, Z.-y. Lu and S. Cui, *J. Am. Chem. Soc.*, 2019, **141**, 9500–9503.
24 M. Guo, X. Sun, J. Chen and T. Cai, *Acta Pharm. Sin. B*, 2021, **11**(8), 2537–2564.
25 V. Yadav, R. Kumar, M. Sharma, A. Dhir and V. K. Bhardwaj, *J. Mol. Struct.*, 2026, **1349**, 143682.
26 G. Bolla and A. Nangia, *Chem. Commun.*, 2016, **52**(54), 8342–8360.
27 J. Pantwalawalkar, N. Kale, S. Nangare, S. Patil, S. Pawar and N. Jadhav, *J. Drug Deliv. Sci. Technol.*, 2024, **104**, 106572.
28 P. S. Panzade and G. R. Shendarkar, *Drug Dev. Ind. Pharm.*, 2020, **46**(10), 1559–1568.
29 L. Liu, M. Liu, Y. Zhang, Y. Feng, L. Wu, L. Zhang, Y. Zhang, Y. Liu, D. Zou and X. Su, *J. Mol. Struct.*, 2022, **1250**, 131848.
30 Y.-N. Zhang, H.-M. Yin, Y. Zhang, D.-J. Zhang, X. Su and H.-X. Kuang, *J. Cryst. Growth*, 2017, **458**, 103–109.
31 X. Pang, Y. Tao, J. Zhang, H. Chen, A. Sun, G. Ren, W. Yang and Q. Pan, *J. Mol. Struct.*, 2023, **1271**, 134079.
32 Y.-N. Zhang, H.-M. Yin, Y. Zhang, D.-J. Zhang, X. Su and H.-X. Kuang, *J. Mol. Struct.*, 2017, **1130**, 199–207.
33 L. Bolus, K. Wang, C. Pask, X. Lai and M. Li, *J. Mol. Struct.*, 2020, **1222**, 128893.
34 L.-x. Liu, X. Su, Y.-n. Zhang, H.-m. Yin, Q. Zhang, Y.-r. Feng, Y.-x. Guo, D.-y. Zou and Y.-l. Liu, *J. Chem. Crystallogr.*, 2020, **51**(3), 363–371.
35 Z. Wang, S. Li, Y. Tao, R. Zheng, S. Yang, D. Yang, S. Wang, L. Zhang, J. Xing, G. Du and Y. Lu, *J. Mol. Struct.*, 2024, **1318**, 139270.
36 Y. Zhu, L. Wang, J. Li, X. Shi, Z. Deng and H. Zhang, *J. Mol. Struct.*, 2025, **1320**, 139719.
37 X. Su, Y. N. Zhang, H. M. Yin, L. X. Liu, Y. Zhang, L. L. Wu, Q. Zhang, C. X. Wang, L. Zhang, Y. J. Zhang and Y. X. Zhang, *J. Mol. Struct.*, 2019, **1177**, 107–116.
38 Y. Yamanoi, *Molecules*, 2024, **29**(3), 576.
39 S. S. Kumar, S. Athimoolam and B. Sridhar, *J. Mol. Struct.*, 2018, **1173**, 951–958.
40 A. D. Cardenal and T. R. Ramadhar, *ACS Cent. Sci.*, 2021, **7**(3), 406–414.
41 R. Schoenlein, T. Elsaesser, K. Holldack, Z. Huang, H. Kapteyn, M. Murnane and M. Woerner, *Philos. Trans. R. Soc. A*, 2019, **377**(2145), 20180384.
42 R. Das, E. Ali and S. B. Abd Hamid, *Rev. Adv. Mater. Sci.*, 2014, **38**(2), 95.
43 R. Nicu, G. Lisa, R. N. Darie-Nita, M. I. Avadanei, A. Bargan, D. Rusu and D. E. Ciolacu, *Gels*, 2024, **10**(8), 523.
44 A. M. Alzahrani, E. S. R. Lasheen and M. A. Rashwan, *Materials*, 2022, **15**(6), 2041.
45 M. I. Gulcebi, S. Gavas and S. M. Sisodiya, *Br. J. Clin. Pharmacol.*, 2025, **91**(8), 2205–2221.
46 Y. Kadioglu, A. Atila, M. Serdar Gultekin and N. Alcan Alp, *Iran. J. Pharm. Res.*, 2013, **12**(4), 659–669.
47 (*a*) CCDC 2526401: Experimental Crystal Structure Determination, 2026, DOI: 10.5517/ccdc.csd.cc2qsxt8; (*b*) CCDC 2526402: Experimental Crystal Structure Determination, 2026, DOI: 10.5517/ccdc.csd.cc2qsxv9.